European Journal of Nuclear Medicine and Molecular Imaging (2022) 49:2482–2492
https://doi.org/10.1007/s00259-022-05731-x

ORIGINAL ARTICLE

Parametric image generation with the uEXPLORER total-body PET/CT system through deep learning

Zhenxing Huang[1,2] · Yaping Wu[3] · Fangfang Fu[3] · Nan Meng[3] · Fengyun Gu[4,5] · Qi Wu[4,5] · Yun Zhou[4] · Yongfeng Yang[1,2] · Xin Liu[1,2] · Hairong Zheng[1,2] · Dong Liang[1,2] · Meiyun Wang[3] · Zhanli Hu[1,2]

Received: 22 October 2021 / Accepted: 13 February 2022 / Published online: 21 March 2022

Abstract

Purpose Total-body dynamic positron emission tomography/computed tomography (PET/CT) provides much sensitivity for clinical imaging and research, bringing new opportunities and challenges regarding the generation of total-body parametric images. This study investigated parametric K_i images directly generated from static PET images without an image-derived input function on a 2-m total-body PET/CT scanner (uEXPLORER) using a deep learning model to significantly reduce the dynamic scanning time and improve patient comfort.

Methods ^{18}F-Fluorodeoxyglucose (^{18}F-FDG) 2-m total-body PET/CT image pairs were acquired for 200 patients (scanned once) with two protocols: one parametric PET image (60 min, 0∼60 min) and one static PET image (10 min, range of 50∼60 min). A deep learning model was implemented to predict parametric K_i images from the static PET images. Evaluation metrics, including the peak signal-to-noise ratio (PSNR), structural similarity index measure (SSIM), and normalized mean square error (NMSE), were calculated for a 10-fold cross-validation assessment. Moreover, image quality was assessed by two nuclear medicine physicians in terms of clinical readings.

Results The synthetic parametric PET images were qualitatively and quantitatively consistent with the reference images. In particular, the global mean SSIM between the synthetic and reference parametric K_i images exceeded 0.9 across all test patients. On the other hand, the overall subjective quality of the synthetic parametric PET images was 4.00 ± 0.45 (the highest possible rating is 5) according to the two expert nuclear medicine physicians.

Conclusion The findings illustrated the feasibility of the proposed technique and its potential to reduce the required scanning duration for 2-m total-body dynamic PET/CT systems. Moreover, this study explored the potential of direct parametric image generation with uEXPLORER. Deep learning technologies may output high-quality synthetic parametric images, and the validation of clinical applications and the interpretability of network models still need further research in future works.

Keywords uEXPLORER · Total-body parametric imaging · Image generation · Deep learning

Zhenxing Huang and Yaping Wu contributed equally to this work.

This article is part of the Topical Collection on Advanced Image Analyses (Radiomics and Artificial Intelligence)

✉ Meiyun Wang
mywang@zzu.edu.cn

✉ Zhanli Hu
zl.hu@siat.ac.cn

[1] Lauterbur Research Center for Biomedical Imaging, Shenzhen Institute of Advanced Technology, Chinese Academy of Sciences, Shenzhen 518055, China

[2] Chinese Academy of Sciences Key Laboratory of Health Informatics, Shenzhen 518055, China

[3] Department of Medical Imaging, Henan Provincial People's Hospital & People's Hospital of Zhengzhou University, Zhengzhou 450003, China

[4] Central Research Institute, United Imaging Healthcare Group, Shanghai 201807, China

[5] Department of Statistics, School of Mathematical Sciences, University College Cork, Cork T12XF62, Ireland

Introduction

As a widely applied standard tool for cancer patient management, positron emission tomography equipped with computed tomography (PET/CT) using ^{18}F-fluoro-deoxyglucose (^{18}F-FDG) is vital for disease diagnosis, progression monitoring, and treatment response [1]. In general, PET is commonly employed in routine clinical practice to obtain static images of radioactivity distributions, and the standardized uptake value (SUV) or its ratio (SUVR) provides a semiquantitative measure of tracer uptake. The SUV of PET is derived at a specific time interval (e.g., 60 min) after tracer injection [2]. However, these measurements may suffer from deception and are affected by several factors, such as body habitus, dietary preparation, and scanning time [3]. In addition, disagreements regarding visual assessments may exist among different readers due to their different levels of expertise. Considered an accurate parameter, the net uptake rate constant K_i is used to quantify PET results and the metabolic rate of glucose derived from kinetic modelling following long-term scanning. A visual assessment can be conducted on high-quality parametric K_i images, and this approach has been proven to reduce interreader disagreement and to curb tracer uptake [4–6]. Compared with SUV analysis, quantitative value analysis demonstrates that a total-body parametric K_i image might achieve an enhanced target-to-background (TBG) ratio and contrast-to-noise ratio (CNR) [7]. Furthermore, whole-body PET parametric K_i images may provide equivalent or superior lesion detectability in comparison with standard-of-care SUVs in clinical oncology [8–10].

The uEXPLORER total-body PET/CT scanner (manufactured by United Imaging Corporation, Shanghai, China), which is equipped with a 194-cm axial field of view (AFOV), acquires entire human body imaging and obtains pathological and physiological information under one bed position [3, 11–15]. Additionally, the acquisition of total-body images with uEXPLORER can be conducted in under 30 s. By contrast, only a part of the human body is utilized in inspection studies because of the limited AFOVs of the traditional PET scanners. Although continuous bed motion (CBM) and step-and-shoot multibed positioning can provide whole-body information for these traditional PET scanners [10, 16], the synchronized acquisition of temporal and spatial information still needs improvement. In total, a total-body PET/CT scanner offers great convenience in obtaining sensitive parametric PET images.

Previous studies [17, 18] revealed different scanning protocols for the generation of parametric K_i images. Wu et al. proposed a parametric K_i image generation approach for FDG PET through dual-time-point scans (5 min per scan) and obtained higher quantification accuracy than that of the relative SUV used in clinical practice [17]. Feng et al. proposed a dual-injection protocol with two scanning periods (0–4 min and 54–60 min postinjection) for acquiring K_i images; the time requirement of this method was greatly reduced, and the results showed strong promise for clinical practice [18]. These works demonstrated that K_i images could be acquired with short scans, similar to static PET images.

On the other hand, deep learning technologies have been introduced into the medical image domain to solve different tasks [19–30], including denoising [20–22, 31], image enhancement [23–25], image reconstruction [26–28, 32], and attenuation correction [29, 30]. Moreover, several works have produced highly promising results in medical image translation tasks with deep learning models. Jiang et al. [33] proposed synthesizing PET/MR (T1-weighted) images from nonattenuation-corrected PET images with Wasserstein generative adversarial networks (WGANs). Yang et al. [34, 35] proposed synthesized models for conversion between CT images and MR images in radiotherapy treatment planning for cancer patients. Moreover, synthetic brain PET is available based on MR images [36]. These deep generative models can play a novel role in medical image translation in terms of visual effects and quantitative results, which reduces hardware dependency while providing referenceable images and saving much computation time.

In this paper, we explore a fast generation approach to predict total-body K_i images without image-derived input function using deep learning technology. A 3D U-Net convolutional neural network (CNN) [20] is implemented to form a mapping function between the static total-body SUV PET images and parametric K_i images of uEXPLORER. Two major challenges when addressing general parametric images through Patlak graphical analysis are the necessity of an image-derived input function (IDIF) and the long acquisition time. Due to the direct generation process of the proposed approach, the image-derived input function is nonessential and acquisition time is significantly reduced in this study.

In terms of reducing the required acquisition time, the benefits of this study are summarized into three categories: (1) the proposed approach improves patient comfort by reducing the scanning time; (2) physical motion artifacts can be significantly avoided due to the use of a shorter scanning protocol; and (3) it can be an alternative for patients who are not suitable for long scans. To the best of our knowledge, this is the first study to directly learn total-body K_i images from static SUV PET images on a total-body PET/CT scanner in the medical image translation domain.

Materials and methods

Participants

Patient data were acquired from Henan Provincial People's Hospital (Zhengzhou, China), and 200 subjects (115 males and 85 females, 55.68 ± 11.09 years old [range of 24–79], body mass indices (BMIs) of 24.65 ± 3.75 kg/m^2 [range of 16.71–41.78]) were scanned from May 2020 to March 2021. Written informed consent was obtained from all subjects before participation in the study. All these patients were scanned once for 60 min, and static SUV PET and parametric K_i images were calculated based on the same scanned raw data.

Static SUV PET image acquisition

Raw data obtained during a 10-min (50~60 min) postinjection period are used to derive static SUV PET images. The PET images are reconstructed via the ordered subset expectation maximization (OSEM) algorithm equipped with a point spread function (PSF). The vendor reconstruction process is implemented with 3 iterations and 20 subsets with time of flight (TOF), attenuation, deadtime, normalization, and decay correction. The reconstructed image size is fixed at 192 ×192 × 673 for a single slice, and the voxel size is 3.125 × 3.125 × 2.886 mm^3. The peak voltage is 120 kVp.

Parametric image acquisition

Raw data obtained 60 min after injection are employed as dynamic data. Similar to the acquisition process for static PET images, dynamic PET images are reconstructed by using the OSEM algorithm equipped with a PSF. The dynamic protocol consists of 98 frames, including 2 s × 50, 10 s × 20, 30 s × 10, 60 s × 10, and 300 s × 8. The Patlak method is used to obtain parametric images via linear least-squares fitting, and data obtained from 20 min postinjection to 60 min postinjection with an image-derived input function are utilized.

Considered the classic graphical PET method, Patlak analysis has been successfully applied for total-body PET scanning [37, 38]. The Patlak model is a standard linear equation related to the input plasma and the measured tissue time activity curves (TACs), and K_i represents the influx constant rate.

CNN implementation

Inspired by Chen et al. [20] and Yin et al. [39], a 3D U-Net CNN framework is utilized in this work in Fig. 1. Briefly, the inputs of this network are static SUV images, and the outputs are estimated parametric K_i images. The standard K_i images derived by the Patlak model are used as the ground truth. Once the deep learning network is trained, the generation model is used to directly create estimated parametric K_i images from the static SUV images.

The inputs and outputs of the 3D U-Net are multislice data with dimensions of $H \times W \times D$, where H and W denote the height (192) and width (192) of the image size, respectively, and D denotes the depth of the continual adjacent multislice data. To reduce the computation time and CUDA memory, we fix D to 3 to extract 3 adjacent slices from the total-body slices. The encoder and decoder portions consist of two-dimensional convolutional layers (using 3 × 3 × 3 filters) and a rectified linear unit (ReLU) activation function. For simple implementation and memory reduction, the number of channels is uniformly set as 32. The down-sampling operation is implemented with a convolution layer

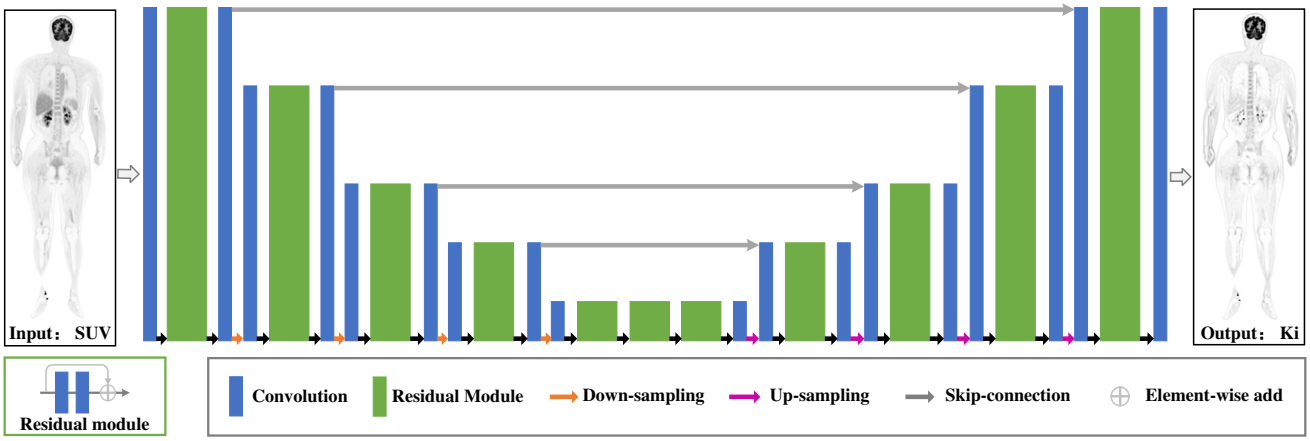

Fig. 1 Schematic of the 3D U-Net framework employed in this work to directly generate total-body parametric PET K_i images from static SUV PET images

with stride=2 without changing the depth of the 3D tensor. In contrast, the upsampling operation is implemented with a deconvolution layer to magnify the image size twice. Skip connections are applied in the residual modules in the central layers to maintain feature information. Among the encoder-decoder components, the combined feature maps from the encoder components and upsampled components are delivered to the corresponding decoder components, thereby increasing information diversity.

For the deep learning model training procedure, cross-validation is adopted, and the process is repeated 10 times to collect as many test results as possible. During each session, 160, 20, and 20 patient data are included in the training, validation, and test processes, respectively. The test data are not visible during the training process. Several data augmentation strategies are introduced, for instance, random flipping (horizontally and vertically), as well as rotation at 90°, 180°, and 270°. The network is trained with a batch size of 16 over 1000 epochs. The mean absolute error (MAE) is selected as the loss function, and the initial learning rate is fixed at 1×10^{-4}. The adaptive moment estimation (ADAM) optimizer is used to optimize the loss function during the training process. Finally, the deep learning model is implemented in the PyTorch framework on an Ubuntu 16.04 system with a Titan 1080Ti GPU.

Evaluation metrics

To evaluate the generated parametric K_i images, subjective and objective metrics are both adopted in this section. Regarding the objective evaluation metrics, the estimated parametric K_i images and ground truths are calculated by using voxel-based analyses. For the output results, we apply several typical evaluation metrics, including the peak signal-to-noise ratio (PSNR), structural similarity index measure (SSIM), and normalized mean square error (NMSE).

The mean square error (MSE) is introduced to calculate the distance between the predicted images and the ground truths; the MSE is formulated as follows:

$$MSE(x,\hat{x}) = \frac{1}{N \times h \times w} \sum_i (x_i - \hat{x}_i)^2, \tag{1}$$

where x denotes the ground truths and $\hat{x}$ denotes the estimated K_i images. N is the number of evaluated images. h and w denote the height and width of x, respectively.

Then, the NMSE is formulated as follows:

$$NMSE = \frac{MSE(x,\hat{x})}{MSE(x,0)} = \frac{\|x-\hat{x}\|_2^2}{\|x\|_2^2}, \tag{2}$$

Based on the definition of the MSE, the PSNR is formulated as follows:

$$PSNR = 10log_{10}\left(\frac{MAX(x)^2}{MSE(x,\hat{x})}\right), \tag{3}$$

where MAX denotes the maximum value of the evaluated image.

Finally, the SSIM is formulated as follows:

$$SSIM = \frac{\left(2\mu_x\mu_{\hat{x}} + C_1\right)\left(2\sigma_{x\hat{x}} + C_2\right)}{\left(\mu_x^2 + \mu_{\hat{x}}^2 + C_1\right)\left(\sigma_x^2 + \sigma_{\hat{x}}^2 + C_2\right)}, \tag{4}$$

where $C_1 = (k_1L)^2$ and $C_2 = (k_2L)^2$. L denotes the pixel scale of the image. k_1 and k_2 are usually fixed at 0.01 and 0.03, respectively. μ_x and $\mu_{\hat{x}}$ denote the average values of x and $\hat{x}$. σ_x^2 and $\sigma_{\hat{x}}^2$ denote the variance of x and $\hat{x}$, and $\sigma_{x\hat{x}}$ denotes their covariance.

Moreover, the data distributions of the local parametric K_i values and the evaluation metrics for different anatomical sites are calculated. In addition, the fused visual results derived from the static PET images and their corresponding parametric K_i images are shown, reflecting the similarity between the generated K_i images and the reference images based on the same static PET images. The region-of-interest (ROI) measurements in the generated images are compared to those of the ground-truth K_i images. The relative differences in each ROI set are found to be normally distributed.

Clinical readings

To obtain a subjective measurement metric, subjective scores are given by clinical nuclear medicine experts with more than 3 years of experience. To evaluate the image quality, the subjective scores ranging from 1 to 5 are assigned for 5 categories: artifact reduction, noise suppression, contrast retention, lesion discrimination, and overall quality. A statistical analysis is conducted on these subjective scores. The generated K_i images and the standard K_i images of each subject are anonymized and presented in random order to 2 clinicians, both of whom had been certified to read total-body parametric K_i images. When clinicians give their subjective scores, the lesion discrimination effect needs to be compared to the corresponding static SUV PET to ensure the correctness of the conclusions. Moreover, some patients (a total of 200) are diagnosed with cancer, such as lung cancer, which increases the diversity of patient health samples. For each presented image, the clinicians assign an image quality score on a 5-point scale: 1 = uninterpretable, 2 = poor, 3 = adequate, 4 = good, and 5 = excellent.

Results

Voxel-based assessment

Figure 2 shows one example of a generated total-body parametric K_i image along with the input static PET image as well as the ground-truth K_i image. Based on the observations derived from three views, including coronal, sagittal, and transverse views, the overall visual effect of the generated image is close to that of the reference image, and most anatomical structure details are present. In addition, high uptake regions can still be effectively represented in the estimated K_i images.

Figure 3 shows the statistical quantitative results of the generated total-body parametric K_i image with respect to the ground-truth K_i image in terms of the PSNR and SSIM. For all cross-validation test data, 10 groups of patients are split, and each group consists of 20 patients. The proposed approach gains superb quantitative results in terms of total-body parametric K_i image generation. The mean PSNR values are distributed over 29.0 db, and the mean SSIM values are distributed over 0.9.

For two selected subjects, the measurement metrics (PSNR, SSIM, and NMSE) are calculated on 6 ROIs, including the brain, neck, lung, abdomen, pelvis, and leg. Table 1 reflects the quantitative results obtained for these two patients. Although the PSNR, SSIM, and NMSE values exhibit differences at different sites, the quantitative results are superb. In particular, the mean SSIM exceeds 0.86 for all generated results. The proposed method achieves a better quantitative performance for the brain site than for other anatomical sites.

Moreover, boxplots are given to illustrate the data distributions of the PSNR, SSIM, and NMSE in Fig. 4. Based on the physicians' experiences, the total-body results are divided into 6 folds (brain, neck, lung, abdomen, pelvis, and leg), and the quantitative metrics are calculated on these folds. For the PSNR, the median value is distributed around 30, and the best performance is in the leg. Note that the median SSIM exceeds 0.94 at 6 sites, and the median NMSE is distributed around 0.15.

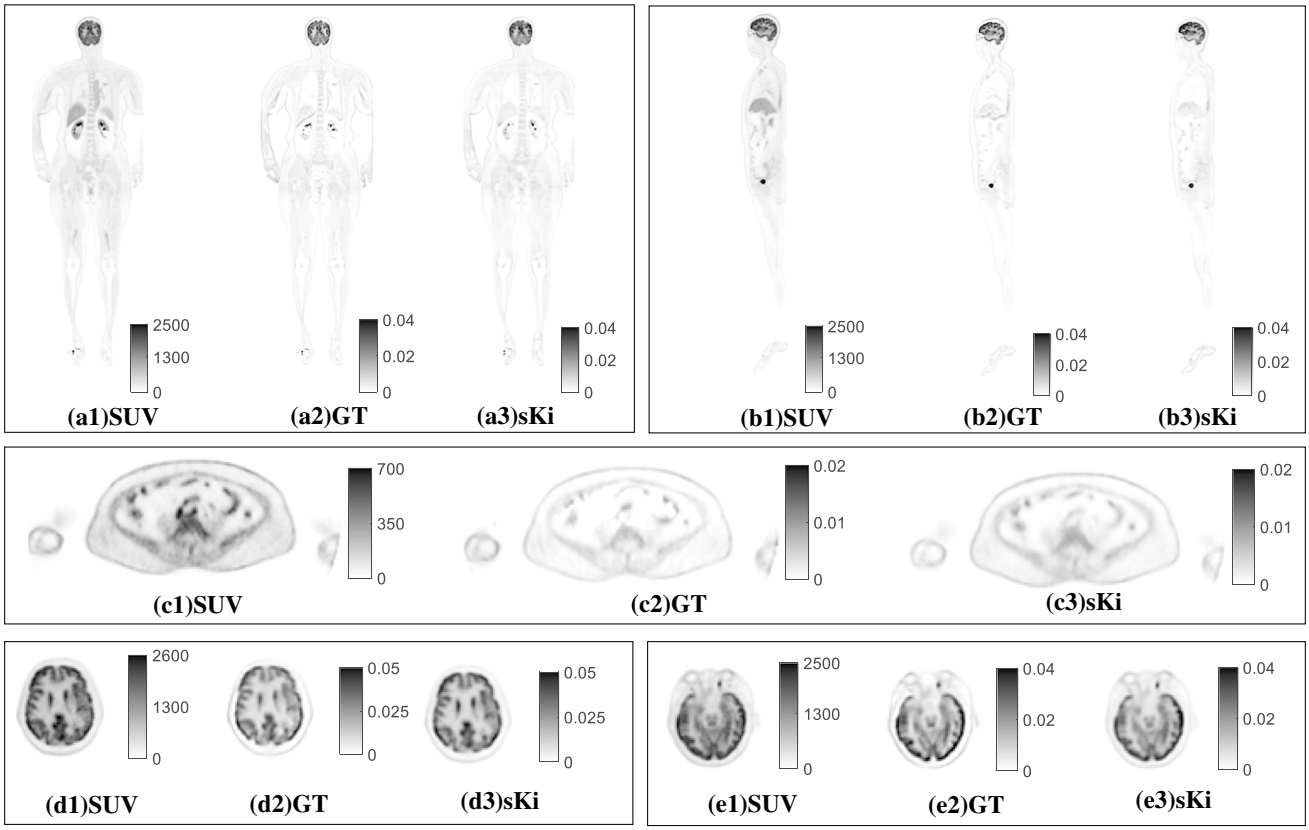

Fig. 2 An example of generated total-body parametric K_i images obtained from different views (coronal, sagittal, and transverse) along with the input static PET image and the ground-truth K_i image. GT denotes the ground-truth K_i image, and sKi denotes the generated *Ki* images

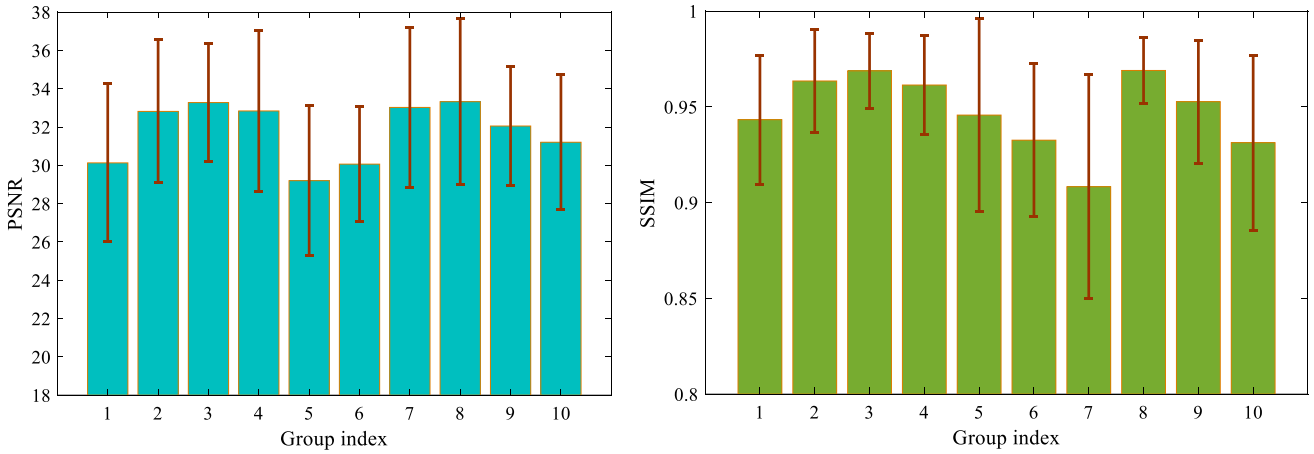

Fig. 3 Statistical quantitative results regarding the total-body parametric K_i images for 10 groups of patients in terms of the PSNR and SSIM. Each group consists of 20 patients

Table 1 Quantitative results (Mean ± Std) obtained on the data of 2 test patients at different anatomical sites in terms of the PSNR, SSIM, and NMSE

Patient ID	Anatomical sites	PSNR	SSIM	NMSE
	Brain	36.61 ± 3.61	0.99 ± 0.01	0.10 ± 0.08
	Neck	30.78 ± 2.41	0.94 ± 0.01	0.13 ± 0.04
1	Lung	29.58 ± 2.21	0.91 ± 0.01	0.26 ± 0.09
(Male)	Abdomen	33.56 ± 2.71	0.95 ± 0.01	0.19 ± 0.12
	Pelvis	34.39 ± 3.85	0.97 ± 0.02	0.10 ± 0.04
	Leg	32.96 ± 2.71	0.98 ± 0.01	0.08 ± 0.03
	Brain	33.28 ± 3.27	0.99 ± 0.01	0.06 ± 0.05
	Neck	29.70 ± 2.52	0.94 ± 0.01	0.14 ± 0.03
2	Lung	28.85 ± 3.64	0.90 ± 0.04	0.19 ± 0.09
(Female)	Abdomen	24.04 ± 2.44	0.87 ± 0.05	0.34 ± 0.08
	Pelvis	31.56 ± 3.67	0.96 ± 0.02	0.13 ± 0.07
	Leg	29.28 ± 2.44	0.97 ± 0.01	0.15 ± 0.04

ROI-based assessment

Quantitative evaluations are performed for the ROIs defined at various anatomical locations, such as the brain, neck, lungs, and abdomen. These regions are selected to represent a range of tracer uptake characteristics. In Fig. 5, a lesion is selected and marked by a red arrow, and the K_i values in a cube ($3 \times 3 \times 3$) surrounding this lesion are counted. The numerical distributions are almost identical among the ROIs of the generated K_i images and ground truths.

To make the results easier to visually distinguish, we introduce the absolute differences for the generated images in Fig. 6. The color bars of the absolute differences are less than the data distributions of the standard K_i images, leading to significant differences. The first row in the coronal direction shows that the proposed method generates the most details. However, several edge structures may not be recovered very well. The second and third rows reveal better restoration performance, and the texture details are well preserved. The obvious metabolic components are reflected in the generated image, which is consistent with the ground truth.

Fusion-based assessment

Generally, the static PET and parameter K_i images are witnessed separately. In several clinical applications, fusion images are very popular for highlighting the contrasts among the objects of concern, for instance, tumors and lesions. In this study, we explore fusion analyses for static PET images and parametric K_i images implemented with Radiant software. Thus, we obtain the ground-truth fusion image (PET + GT) and the comparison fusion image (PET + sKi). PET denotes the static input PET image, GT denotes the reference K_i image, and *sKi* denotes the generated image. In Fig. 7, the compared image is quite similar to the reference image. Specifically, the morphological manifestations of the high metabolic regions are consistent. Three coronal and transverse slices are selected, and the results show similar effects. In particular, the fusion images at the brain site show similar high metabolic areas marked by bright pseudocolors.

Clinical readings

To clearly illustrate the clinical readings, subjective metrics are introduced to evaluate their visual quality. The subjective scores are provided by two experts with adequate clinical experience. Subjective scores ranging from 1 to 5 are assigned to the generated K_i images and ground-truth images of 20 patients randomly selected from the test samples. Figure 8 presents the subjective results in terms of five aspects

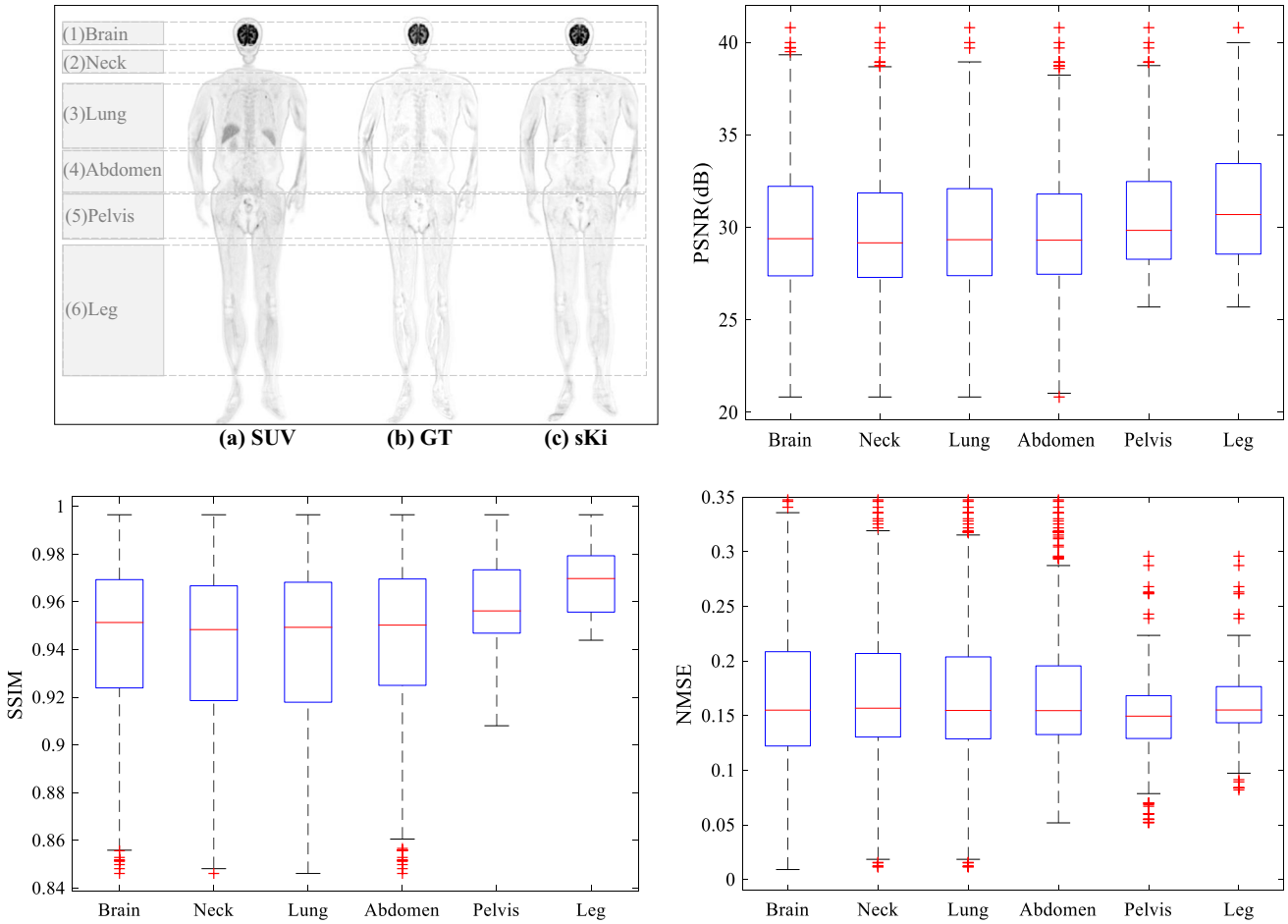

Fig. 4 Box plots of the data distributions at 6 ROIs for different anatomical sites of a patient in terms of the PSNR, SSIM, and NMSE

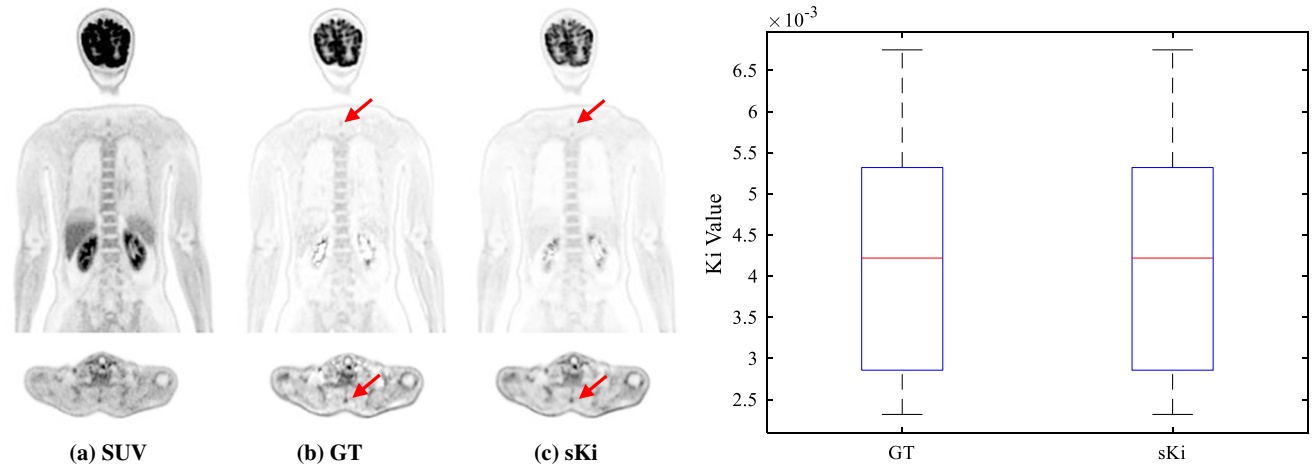

Fig. 5 Data distributions of the K_i values on a tumor for the ground truth and generated image (sKi)

(artifact reduction, noise suppression, contrast retention, lesion discrimination, and overall quality). The quantitative subjective scores provided by the two expert nuclear medicine physicians are 4.00 ± 0.45 for overall quality, and the five aspects are distributed around 4.00. The subjective results support the superiority of the results produced

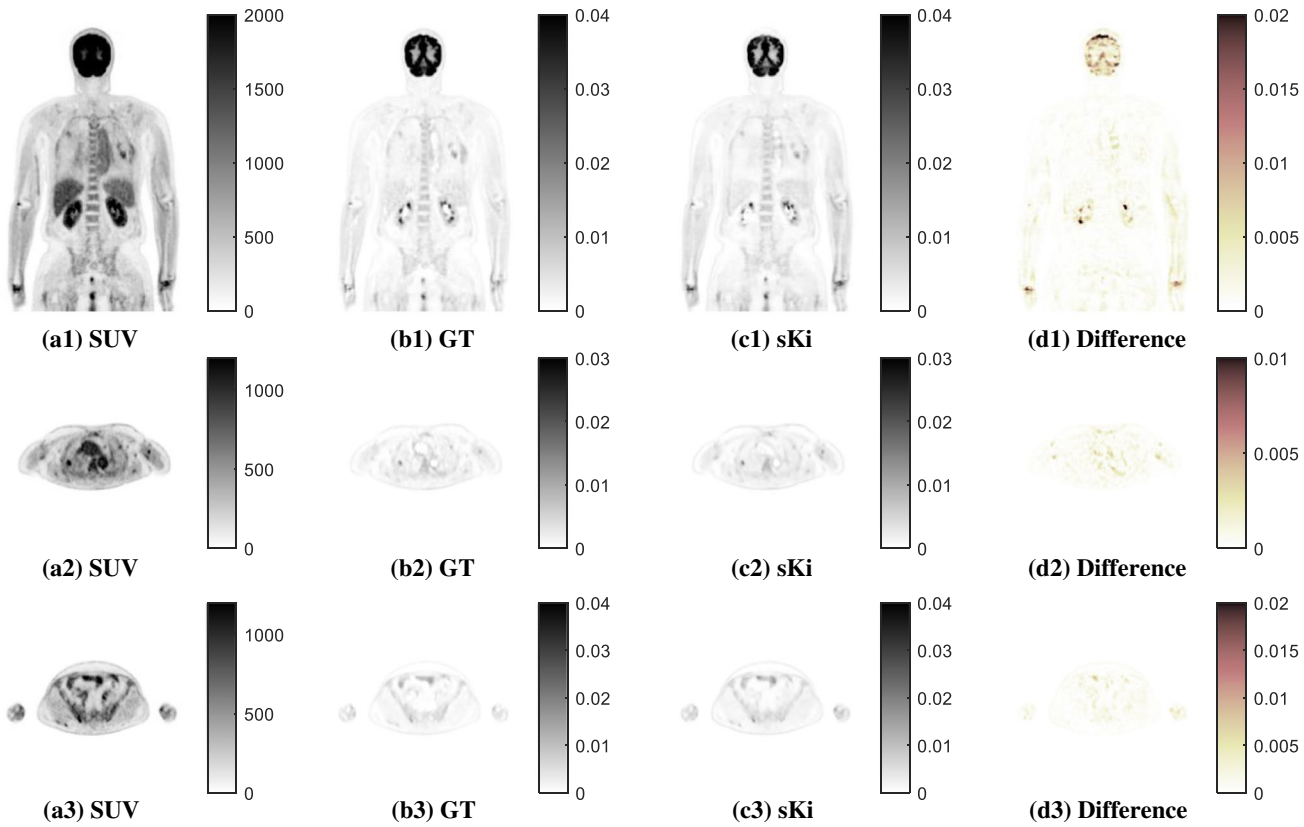

Fig. 6 Absolute differences between the generated K_i images and the ground truths. The first column shows the input static PET images; the second column shows the reference K_i images; the third column presents the generated K_i images; and the last column shows the absolute differences between the generated and reference K_i images

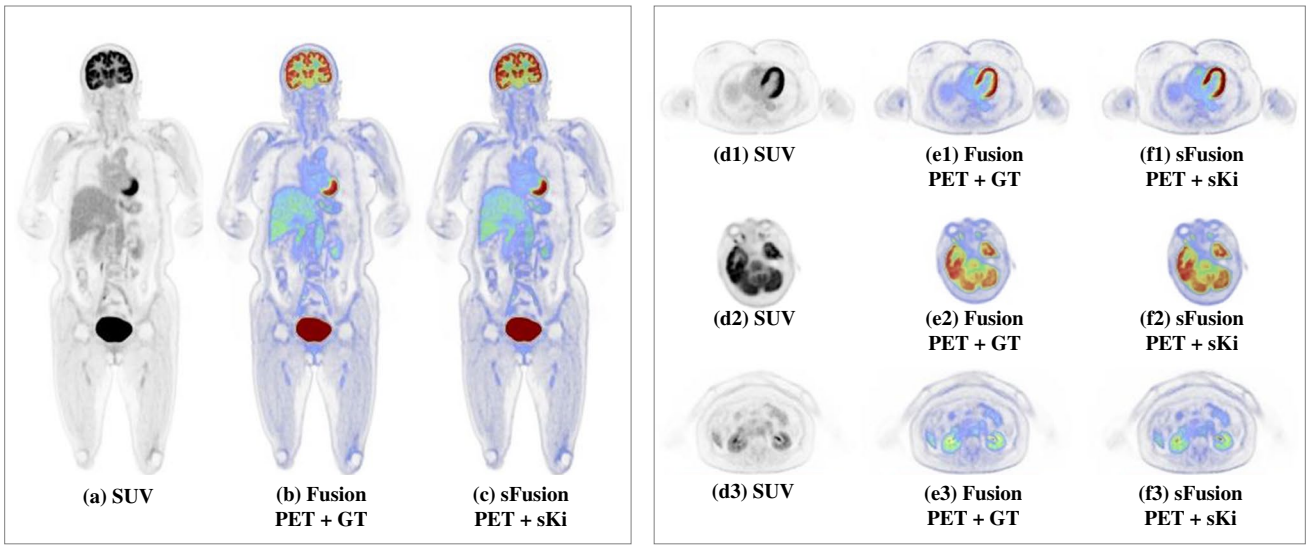

Fig. 7 Comparison between the fused images in the coronal and transverse positions

by the proposed method in comparison with referenced images. In particular, the generated results based on deep learning methods gain smoother images, thereby reducing noise interference and achieving better performance in terms of artifact reduction and noise suppression. Furthermore, the quantitative subjective results in Table 2 show that the

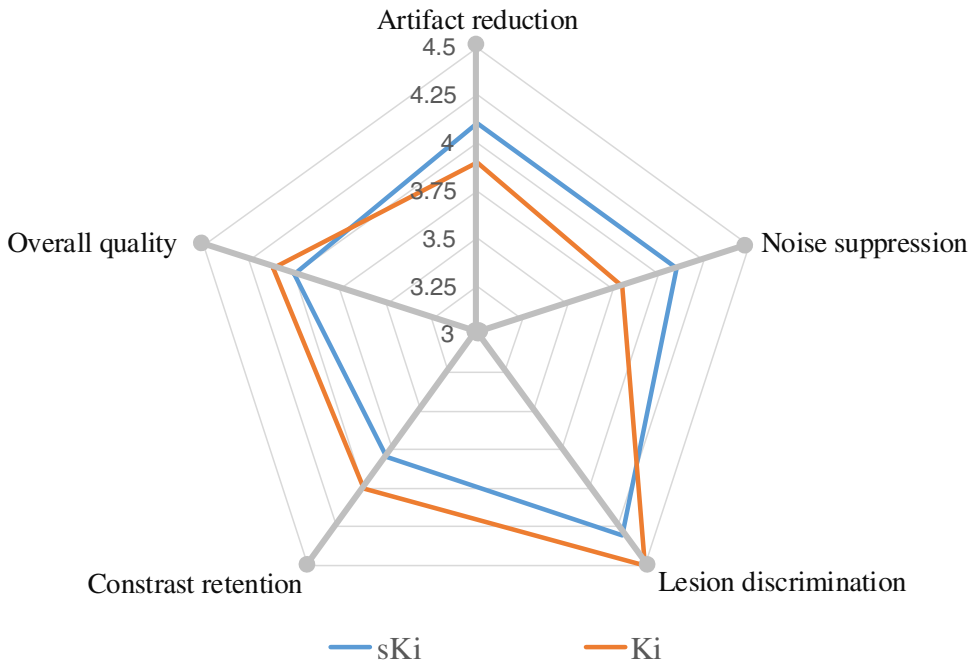

Fig. 8 Radar plot of the subjective quantitative results for the generator K_i images and the ground truths in terms of five aspects. The highest subjective rate for the five clinical aspects is 5. The orange box shows the mean subjective scores provided by two oncologists for the reference and synthetic K_i images

Table 2 Quantitative subjective results (Mean ± Std) provided by 2 oncologists in terms of clinical readings

Oncologist ID	Aspects	sKi	Ki
1	Artifact reduction	4.20 ± 0.40	3.80 ± 0.40
	Noise suppression	4.20 ± 0.40	3.80 ± 0.40
	Lesion discrimination	4.10 ± 0.70	4.30 ± 0.64
	Contrast retention	3.70 ± 0.46	3.90 ± 0.70
	Overall quality	3.90 ± 0.30	4.00 ± 0.45
2	Artifact reduction	3.90 ± 0.30	3.70 ± 0.46
	Noise suppression	3.90 ± 0.30	3.80 ± 0.40
	Lesion discrimination	4.30 ± 0.64	4.50 ± 0.67
	Contrast retention	3.60 ± 0.49	3.70 ± 0.64
	Overall quality	4.10 ± 0.30	4.20 ± 0.60

generated K_i images may exhibit lower contrast retention, but they achieve better artifact reduction and noise suppression performance across the five subjective evaluation metrics.

Discussion

We developed a fast and effective deep learning-based model for estimating total-body parametric images directly from PET emission data. Evaluations conducted on real patient data showed that the proposed method could produce parametric images that were consistent with reference images derived by Patlak plots and was able to provide accurate fusion images. This development could have a direct benefit in terms of reducing the scanning time to improve patient comfort. We found that the proposed approach produced slightly better quantitative results for male subjects than female subjects. This might have been caused by the anatomical differences between females and males. The training phase took approximately 8 h on a Titan 1080Ti GPU. In the testing phase, it took less than 1 s to generate a parametric K_i image from static SUV PET data.

Based on our observations, the generated parametric K_i images contained certain static PET structural information because the generated images were learned from the input static SUV PET sources, and much original image information was preserved. Generally, parametric K_i images have better rendering effects on lesions than static PET images. For these lesions, both parametric K_i and static PET images represent the characteristics of lesions. Thus, the generated K_i images, which could be considered fused images, may show functional information from two components simultaneously for static and parametric images. When clinicians conduct diagnoses, such as lesion discrimination, it is suggested to compare the generated K_i images to the corresponding static SUV PET images to ensure the correctness of the conclusions.

The proposed deep learning models could directly produce high-quality synthetic parametric images, and a GAN framework can be considered to improve the generation performance. Although the proposed method performed well in terms of various evaluation metrics, further research might focus on validation for clinical applications. In future studies, more patient cases should be incorporated into the deep learning-based training process, and a larger number of female patients should be included for both training and

evaluation. Moreover, extra prior constraints for parametric models may need to be further researched to maintain the medical integrity of generated data. The parametric images can be derived from dynamic PET images, and deep learning technology can be integrated into the calculation of progress priors, which would greatly improve the interpretability of the network.

Conclusion

In this work, we explored a fast deep learning method for generating total-body parametric K_i images from static SUV images without an image-derived input function. The performance of the proposed method is evaluated through subjective and objective measurement metrics calculated on 200 patient data, which were collected with a 2-m total-body PET/CT scanner (uEXPLORER). The results demonstrated the effectiveness of accurate parametric K_i image estimation implemented with deep learning-based technology, which has the potential to reduce the scanning time to improve patient comfort. Although the proposed method performed well in quantitative evaluations, it requires much validation in clinical applications. Further research should be considered in future works to improve the capabilities of the current model; for instance, network implementation and the joint prior information of the parametric image derivation procedure can be studied to significantly improve the interpretability of neural network models.

Author Contributions Z. Huang, Y. Wu, M. Wang, and Z. Hu had full access to all the study data and take full responsibility for its integrity. Z. Huang and Z. Hu conceptualized and designed the study. Y. Wu and M. Wang acquired the data. Z. Huang, Y. Wu, F. Fu, N. Meng, X. Liu, and H. Zheng analyzed and interpreted the data. Z. Huang, Y. Wu, and F. Gu drafted the manuscript. Z. Huang, Q. Wu, D. Liang, and Y. Yang performed the statistical analysis. Z. Huang and Z. Hu secured funding. All the authors critically revised the manuscript.

Funding This work was supported by the National Natural Science Foundation of China (32022042, 81871441, and 62101540), the Shenzhen Excellent Technological Innovation Talent Training Project of China (RCJC20200714114436080), the Natural Science Foundation of Guangdong Province in China (2020A1515010733), and the Chinese Academy of Sciences Key Laboratory of Health Informatics in China (2011DP173015).

Availability of data and material The dataset used and/or analyzed during the current study is available from the corresponding author on reasonable request.

Declarations

Ethics approval The Ethics Committee of Henan Provincial People's Hospital & the People's Hospital of Zhengzhou University approved this study (approval number: IRB 2020-127).

Consent to participate Written informed consent for imaging was obtained from all participants or an authorized surrogate decision maker.

Conflict of interest Fengyun Gu, Qi Wu, and Yun Zhou are employees of the United Imaging Healthcare group. The other authors have no conflicts of interest.

References

1. Lammertsma AA. Forward to the past: the case for quantitative pet imaging. J Nucl Med. 2017;58(7):1019–24.
2. Tomasi G, Turkheimer F, Aboagye E. Importance of quantification for the analysis of pet data in oncology: review of current methods and trends for the future. Mol Imaging Biol. 2012;14(2):131–46.
3. Wang Y, Li E, Cherry SR, Wang G. Total-body pet kinetic modeling and potential opportunities using deep learning. PET Clin. 2021;16(4):613–25.
4. Collij LE, Konijnenberg E, Reimand J, Ten Kate M, Den Braber A, Alves IL, Zwan M, Yaqub M, van Assema DM, Wink AM, et al. Assessing amyloid pathology in cognitively normal subjects using 18f-flutemetamol pet: comparing visual reads and quantitative methods. J Nucl Med. 2019;60(4):541–7.
5. Peretti DE, Vállez García D, Reesink FE, van der Goot T, De Deyn PP, de Jong BM, Dierckx RA, Boellaard R. Relative cerebral flow from dynamic pib scans as an alternative for fdg scans in alzheimer's disease pet studies. PloS ONE. 2019;14(1):e0211000.
6. Leahy R, Boellaard R, Zaidi H. Whole-body parametric pet imaging will replace conventional image-derived pet metrics in clinical oncology. Med Phys. 2018;45(12):5355–8.
7. Zhuang M, Karakatsanis NA, Dierckx RA, Zaidi H. Quantitative analysis of heterogeneous [18 f] fdg static (suv) vs. patlak (ki) whole-body pet imaging using different segmentation methods: a simulation study. Mol Imaging Biol. 2019;21(2):317–27.
8. Fahrni G, Karakatsanis NA, Di Domenicantonio G, Garibotto V, Zaidi H. Does whole-body patlak 18 f-fdg pet imaging improve lesion detectability in clinical oncology? Eur Radiol. 2019;29(9):4812–21.
9. Chen Y, Li L, Yu X, Wang J, Wang Y, Huang G, Liu J. Is dynamic total-body pet imaging feasible in the clinical daily practice? 2021.
10. Zaker N, Kotasidis F, Garibotto V, Zaidi H. Assessment of lesion detectability in dynamic whole-body pet imaging using compartmental and patlak parametric mapping. Clin Nucl Med. 2020;45(5):e221–31.
11. Zhang X, Xie Z, Berg E, Judenhofer MS, Liu W, Xu T, Ding Y, Lv Y, Dong Y, Deng Z, et al. Total-body dynamic reconstruction and parametric imaging on the uEXPLORER. J Nucl Med. 2020;61(2):285–91.
12. Liu G, Xu H, Hu P, Tan H, Zhang Y, Yu H, Li X, Shi H. Kinetic metrics of 18 f-fdg in normal human organs identified by systematic dynamic total-body positron emission tomography. Eur J Nucl Med Mol Imaging. 2021;1–10.
13. Lan X, Fan K, Li K, Cai W. Dynamic pet imaging with ultra-low-activity of 18 f-fdg: unleashing the potential of total-body pet. 2021.
14. Zhang X, Cherry SR, Xie Z, Shi H, Badawi RD, Qi J. Subsecond total-body imaging using ultrasensitive positron emission tomography. Proc Natl Acad Sci. 2020;117(5):2265–7.
15. Tan H, Sui X, Yin H, Yu H, Gu Y, Chen S, Hu P, Mao W, Shi H. Total-body pet/ct using half-dose fdg and compared with conventional pet/ct using full-dose fdg in lung cancer. Eur J Nucl Med Mol Imaging. 2021;48(6):1966–75.

16. Hu J, Panin V, Smith AM, Spottiswoode B, Shah V, von Gall CC, Baker M, Howe W, Kehren F, Casey M, et al. Design and implementation of automated clinical whole body parametric pet with continuous bed motion. IEEE Trans Radiat Plasma Med Sci. 2020;4(6):696–707.
17. Wu J, Liu H, Ye Q, Gallezot J-D, Naganawa M, Miao T, Lu Y, Chen M-K, Esserman DA, Kyriakides TC, et al. Generation of parametric ki images for fdg pet using two 5-min scans. Med Phys. 2021.
18. Feng T, Wu Y, Zhao Y, Xu T, Fu F, Huang Z, Meng N, Li H, Shao F, Wang M. Whole-body parametric imaging of fdg pet using uexplorer with reduced scan time. J Nucl Med. 2021.
19. Schaefferkoetter J, Yan J, Moon S, Chan R, Ortega C, Metser U, Berlin A, Veit-Haibach P. Deep learning for whole-body medical image generation. Eur J Nucl Med Mol Imaging. 2021;1–10.
20. Chen KT, Schürer M, Ouyang J, Koran MEI, Davidzon G, Mormino E, Tiepolt S, Hoffmann K-T, Sabri O, Zaharchuk G, et al. Generalization of deep learning models for ultra-low-count amyloid pet/mri using transfer learning. Eur J Nucl Med Mol Imaging. 2020;47(13):2998–3007.
21. Cui J, Gong K, Guo N, Wu C, Meng X, Kim K, Zheng K, Wu Z, Fu L, Xu B, et al. Pet image denoising using unsupervised deep learning. Eur J Nucl Med Mol Imaging. 2019;46(13):2780–9.
22. Huang Z, Liu X, Wang R, Chen Z, Yang Y, Liu X, Zheng H, Liang D, Hu Z. Learning a deep cnn denoising approach using anatomical prior information implemented with attention mechanism for low-dose ct imaging on clinical patient data from multiple anatomical sites. IEEE J Biomed Health Inform. 2021;25(9):3416–27.
23. Chen KT, Toueg TN, Koran MEI, Davidzon G, Zeineh M, Holley D, Gandhi H, Halbert K, Boumis A, Kennedy G, et al. True ultra-low-dose amyloid pet/mri enhanced with deep learning for clinical interpretation. Eur J Nucl Med Mol Imaging. 2021;1–10.
24. Sanaat A, Shiri I, Arabi H, Mainta I, Nkoulou R, Zaidi H. Deep learning-assisted ultra-fast/low-dose whole-body pet/ct imaging. Eur J Nucl Med Mol Imaging. 2021;1–11.
25. Huang Z, Liu X, Wang R, Chen J, Lu P, Zhang Q, Jiang C, Yang Y, Liu X, Zheng H, et al. Considering anatomical prior information for low-dose ct image enhancement using attribute-augmented wasserstein generative adversarial networks. Neurocomputing. 2021;428:104–15.
26. Gong K, Catana C, Qi J, Li Q. Pet image reconstruction using deep image prior. IEEE Trans Med Imaging. 2018;38(7):1655–65.
27. Gong K, Guan J, Kim K, Zhang X, Yang J, Seo Y, El Fakhri G, Qi J, Li Q. Iterative pet image reconstruction using convolutional neural network representation. IEEE Trans Med Imaging. 2018;38(3):675–85.
28. Reader AJ, Corda G, Mehranian A, da Costa-Luis C, Ellis S, Schnabel JA. Deep learning for pet image reconstruction. IEEE Trans Radiat Plasma Med Sci. 2020;5(1):1–25.
29. Gong K, Han PK, Johnson KA, El Fakhri G, Ma C, Li Q. Attenuation correction using deep learning and integrated ute/multi-echo dixon sequence: evaluation in amyloid and tau pet imaging. Eur J Nucl Med Mol Imaging. 2021;48(5):1351–61.
30. Shi L, Onofrey JA, Liu H, Liu Y-H, Liu C. Deep learning-based attenuation map generation for myocardial perfusion spect. Eur J Nucl Med Mol Imaging. 2020;47(10).
31. Huang Z, Chen Z, Chen J, Lu P, Quan G, Du Y, Li C, Gu Z, Yang Y, Liu X, et al. Danet: dose-aware network embedded with dose-level estimation for low-dose ct imaging. Phys Med Biol. 2021;66(1):015005.
32. Zhang Y, Hu D, Zhao Q, Quan G, Liu J, Liu Q, Zhang Y, Coatrieux G, Chen Y, Yu H. Clear: comprehensive learning enabled adversarial reconstruction for subtle structure enhanced low-dose ct imaging. IEEE Trans Med Imaging. 2021;40(11):3089–101.
33. Jiang C, Zhang X, Zhang N, Zhang Q, Zhou C, Yuan J, He Q, Yang Y, Liu X, Zheng H, et al. Synthesizing pet/mr (t1-weighted) images from non-attenuation-corrected pet images. Phys Med Biol. 2021.
34. Yang H, Sun J, Carass A, Zhao C, Lee J, Prince JL, Xu Z. Unsupervised mr-to-ct synthesis using structure-constrained cyclegan. IEEE Trans Med Imaging. 2020;39(12):4249–61.
35. Yang H, Lu X, Wang S-H, Lu Z, Yao J, Jiang Y, Qian P. Synthesizing multi-contrast mr images via novel 3d conditional variational auto-encoding gan. Mob Netw Appl. 2021;26(1):415–24.
36. Hu S, Shen Y, Wang S, Lei B. Brain mr to pet synthesis via bidirectional generative adversarial network. In: International conference on medical image computing and computer-assisted intervention. Springer; 2020. pp 698–707
37. Karakatsanis NA, Zhou Y, Lodge MA, Casey ME, Wahl RL, Zaidi H, Rahmim A. Generalized whole-body patlak parametric imaging for enhanced quantification in clinical pet. Phys Med Biol. 2015;60(22):8643.
38. Karakatsanis NA, Casey ME, Lodge MA, Rahmim A, Zaidi H. Whole-body direct 4d parametric pet imaging employing nested generalized patlak expectation-maximization reconstruction. Phys Med Biol. 2016;61(15):5456.
39. Yin X, Zhao Q, Liu J, Yang W, Yang J, Quan G, Chen Y, Shu H, Luo L, Coatrieux J-L. Domain progressive 3d residual convolution network to improve low-dose ct imaging. IEEE Trans Med Imaging. 2019;38(12):2903–13.